

M(bipyridine)V₄O₁₀ (M = Cu, Ag): Hybrid Analogues of Low-Dimensional Reduced Vanadates

Bangbo Yan and Paul A. Maggard*

Department of Chemistry, North Carolina State University, Raleigh, North Carolina 27695-8204

Received April 17, 2007

New hybrid layered vanadates, M(bpy)V₄O₁₀ (I, M = Cu⁺; II, M = Ag⁺; bpy = 4,4'-bipyridine), were prepared from hydrothermal reactions at 220–230 °C, and their structures were characterized by single-crystal X-ray diffraction [I, *P*2₁/*c* (No. 14), *Z* = 4, *a* = 3.6154(3) Å, *b* = 21.217(1) Å, *c* = 20.267(1) Å, and β = 90.028(3)°; II, *P*1̄ (No. 2), *Z* = 2, *a* = 3.5731(4) Å, *b* = 10.429(1) Å, *c* = 21.196(2) Å, α = 89.031(5)°, β = 89.322(5)°, and γ = 85.546(5)°]. The structures of I and II are closely related, though not isostructurally, with both containing partially reduced V₄O₁₀[−] layers that are constructed from zigzag chains of edge-sharing VO₅ tetragonal pyramids. Neighboring zigzag chains within a layer condense via shared vertices and alternate between versions containing V^{4.5+} and V⁵⁺ ions, such that two out of four symmetry-unique V atoms are reduced by a half-electron on average. The interlayer spaces contain unusual M(bpy)⁺ chains formed from the coordination of two bridging bpy ligands to Ag⁺/Cu⁺ in a nearly linear fashion and each with a third bond to a single apical O atom of the reduced (V^{4.5+}) VO₅ tetragonal pyramids. Both I and II are stable until ~350–400 °C in O₂, at which point the ligands are liberated to yield the purely inorganic M_xV₄O₁₀ (M = Ag, Cu) solids. The electrical conductivities of both compounds show a temperature dependence that is consistent with Mott's variable-range-hopping model for randomly localized electrons. Magnetic susceptibilities of both I and II can be fitted to a Curie–Weiss expression (θ = −25 and −31 K, respectively; *C* ~ 0.40 emu·mol^{−1}·K for both) at higher temperatures and one unpaired spin per formula. However, at below ~12–18 K, both show evidence for an antiferromagnetic transition that can be fitted well to the Heisenberg linear antiferromagnetic chain model. These results are analyzed with respect to related reduced vanadates and help to provide new structure–property insights for strongly correlated electron systems.

Introduction

The solid-state chemistry of layered vanadates has revealed a remarkable diversity and significant degree of structural flexibility found both within their layers and in the incorporation of interlayer guest species.^{1,2} For example, wide varieties of small organic molecules,^{3–6} as well as polymers,^{7,8} have been incorporated as guests between vanadate layers (V_xO_y^{*n*−}), including many types of alkylamines and aromatic amines and that can also coordinate to late transition-metal cations such as Co²⁺, Ni²⁺, Cu²⁺, or Zn²⁺.^{9–17} This expansive chemistry discovered for vanadate

layers arises from the number of possible vanadium coordination geometries, e.g., VO₄, VO₅, and VO₆, and their strong tendency to condense into layered formats with a

* To whom correspondence should be addressed. E-mail: paul_maggard@ncsu.edu. Phone: (+1) 919-515-3616. Fax: (+1) 919-515-5079.

- (1) Hagrman, P. J.; Finn, R. C.; Zubieta, J. *J. Solid State Sci.* **2001**, *3*, 745–774.
- (2) Chirayil, T.; Zavalij, P. Y.; Whittingham, M. S. *Chem. Mater.* **1998**, *10*, 2629–2640.
- (3) (a) Nazar, L. F.; Koene, B. E.; Britten, J. F. *Chem. Mater.* **1996**, *8*, 327–329. (b) Koene, B. E.; Taylor, N. J.; Nazar, L. F. *Angew. Chem., Int. Ed.* **1999**, *38*, 2888–2891.

- (4) (a) Chirayil, T. G.; Boylan, E. A.; Mamak, M.; Zavalij, P. Y.; Whittingham, M. S. *Chem. Commun.* **1997**, 33–34. (b) Chirayil, T.; Zavalij, P. Y.; Whittingham, M. S. *J. Mater. Chem.* **1997**, *7* (11), 2193–2195. (c) Zavalij, P. Y.; Chirayil, T.; Whittingham, M. S. *Acta Crystallogr., Sect. C* **1997**, *C53* (7), 879–881. (d) Zavalij, P. Y.; Whittingham, M. S.; Boylan, E. A.; Pecharsky, V. K.; Jacobson, R. A. *Z. Kristallogr.* **1996**, *211* (7), 464. (e) Chen, R.; Zavalij, P. Y.; Whittingham, M. S.; Greedan, J. E.; Raju, N. P.; Bieringer, M. J. *Mater. Chem.* **1999**, *9*, 93–100.
- (5) (a) Zhang, Y.; O'Connor, C. J.; Clearfield, A.; Haushalter, R. C. *Chem. Mater.* **1996**, *8* (3), 595–597. (b) Zhang, Y.; Haushalter, R. C.; Clearfield, A. *Chem. Commun.* **1996**, 1055–1056. (c) Zhang, Y.; Warren, C. J.; Haushalter, R. C. *Chem. Mater.* **1998**, *10*, 1059–1064. (d) Zhang, Y.; Haushalter, R. C.; Clearfield, A. *Inorg. Chem.* **1996**, *35* (17), 4950–4956.
- (6) (a) Riou, D.; Férey, G. J. *J. Solid State Chem.* **1995**, *120*, 137–145. (b) Riou, D.; Férey, G. J. *Inorg. Chem.* **1995**, *34*, 6520–6523. (c) Riou, D.; Férey, G. J. *J. Solid State Chem.* **1996**, *124*, 151–154. (d) Riou, D.; Roubeau, O.; Bouhedja, L.; Livage, J.; Férey, G. *Chem. Mater.* **2000**, *12*, 67–72.
- (7) Liu, Y. J.; Degroot, D. C.; Schindler, J. L.; Kannewurf, C. R.; Kanatzidis, M. G. *Adv. Mater.* **1993**, *5*, 369–372.

variety of orientations and structural patterns via the sharing of edges and/or vertices. As a result, interlayer guest species may exert a significant structure-guiding influence on the vanadate layers via hydrogen bonding and covalent interactions to the terminal O atoms, to influence the V–O–V connectivity as well as the orientation of vanadate polyhedra. Coupled to this flexibility is the accessibility of reduced vanadium oxidation states during their hydrothermal preparation, leading to new possibilities of intriguing quantum-spin systems that are currently the subject of intense research in condensed layered vanadates.¹⁸

Our research efforts have focused on the synthesis of reduced layered vanadates that are hybrid oxide/organic analogues of condensed vanadates with spin gaps and/or extended spin lattices such as ladders. While these layered vanadates have attracted attention for their remarkable magnetic properties, in contrast, among the related hybrid vanadates nearly all of the studied systems have involved simple, isolated spin dimers, such as in LV_3O_7 [$\text{L} = \text{C}_4\text{H}_8\text{NH}_2$, $(\text{CH}_3)_2\text{NH}_2$, $\text{C}_5\text{H}_{10}\text{NH}_2$, $\text{C}_5\text{H}_5\text{NH}$, and $\text{N}(\text{CH}_3)_4$],^{19,20} $(\text{en})_2\text{ZnV}_6\text{O}_{14}$,^{9,21} and $(\text{C}_6\text{H}_{14}\text{N}_2)\text{V}_6\text{O}_{14}\cdot\text{H}_2\text{O}$,^{3a} or the spin tetramer, such as in $[\text{H}_2\text{N}(\text{CH}_2)_4\text{NH}_2]\text{V}_4\text{O}_9$.²² Many of these exhibit values of the exchange coupling constants that are as large as those between oxide-bridged Cu atoms in the cuprate layers of high- T_c superconductors.²¹ Therefore, there is a significant untapped potential yet to be realized in expanding the diversity of layered vanadates toward more flexible hybrid structures containing extended spin lattices. The incorporation of interlayer ligands and secondary transition metals that will coordinate to and influence the atomic and electronic structures of the vanadate layers would lead to a broader range of functionality and flexibility in which to more deeply probe their magnetic properties. Towards this goal, we have targeted the synthesis of different layered metal oxides also containing metal–organic layers,^{23–26} including most notably the reduced layered hybrids $\text{M}(\text{pyz})\text{V}_4\text{O}_{10}$ (*M*

= Co, Ni, Zn; pyz = pyrazine).²⁷ The $\text{M}(\text{pyz})\text{V}_4\text{O}_{10}$ series demonstrated for the first time that close hybrid analogues of a layered vanadate with a spin gap, i.e., NaV_2O_5 ($T_c \sim 35$ K),²⁸ could be synthesized and the electron–electron interactions within the vanadate layer suppressed (*M* = Co, Ni) or altered (*M* = Zn; $T_c \sim 22$ K) by interlayer metal–organic networks.

Presented herein are two new layered and reduced hybrid vanadates, $\text{M}(\text{bpy})\text{V}_4\text{O}_{10}$ (**I**, *M* = Cu⁺; **II**, *M* = Ag⁺; bpy = 4,4'-bipyridine), that have been synthesized using hydrothermal methods and that contain partially reduced vanadate layers. Both contain vanadate layers that are remarkably similar to that found in LiV_2O_5 ,²⁹ a quasi-1D spin system, in which zigzag chains of edge-shared VO_5 polyhedra condense into a layer and the neighboring chains alternate between V^{5+} and reduced $\text{V}^{4.5+}$ cations. Further, new structural insights are gained into the effects that interlayer $\text{Ag}(\text{bpy})^+$ and $\text{Cu}(\text{bpy})^+$ chains have upon the topology and dimensions of the $\text{V}_4\text{O}_{10}^-$ layer. Compounds **I** and **II** were further characterized by thermogravimetric analysis (TGA), electrical conductivity, and magnetic susceptibility measurements, and the results are described and analyzed herein.

Experimental Section

Materials. V_2O_5 (99.99%, Alfa Aesar), Ag_2O (99%, Aldrich), $\text{Cu}(\text{OH})_2$ (99%, Alfa Aesar), and 4,4'-bipyridine (bpy; 98+%, Alfa Aesar) were used as received. A reagent amount of deionized water was also used in the syntheses.

Synthesis. The synthesis of $\text{Cu}(\text{bpy})\text{V}_4\text{O}_{10}$ (**I**) was performed by mixing V_2O_5 (0.0484 g, 0.266 mmol), $\text{Cu}(\text{OH})_2$ (0.0129 g, 0.132 mmol), bpy (0.0421 g, 0.270 mmol), and deionized water (1.97 g, 0.109 mol) inside a heat-sealed Teflon bag. The Teflon bags were made by heating sealing FEP Teflon film (American Durafilm, 0.005 in. thick) and used in order to separate the reactants of multiple synthetic trials within one reaction vessel. The reaction containers were placed inside a Teflon-lined autoclave, backfilled with ~33% deionized water, sealed, and heated to 220 °C for 3 days before being allowed to radiatively cool to room temperature within a few hours. No evidence of leakage (i.e., color or volume changes) in the Teflon bags was found under these conditions. The products were filtered, washed with water, and dried at 40 °C. The two predominant crystal morphologies included mostly small needle crystals together with long platelet crystals that were both dark red. A small amount of an uncharacterized yellow solid was removed by washing. A powder X-ray diffraction (PXRD) analysis of the washed product confirmed that **I** is obtained in high purity from the reaction, as determined subsequent to the X-ray analysis on the single crystals (below). Longer hydrothermal reaction times of up to 5 days result in the highest purities (>99% by PXRD) and in mass percent yields up to ~76% based on V.

The synthesis of $\text{Ag}(\text{bpy})\text{V}_4\text{O}_{10}$ (**II**) was performed in a fashion similar to that described above for **I**, with the substitution of a

- (8) Kanatzidis, M. G.; Wu, C. G. *J. Am. Chem. Soc.* **1989**, *111*, 4139.
 (9) Zhang, Y.; DeBord, J. R. D.; O'Connor, C. J.; Haushalter, R. C.; Clearfield, A.; Zubieta, J. *Angew. Chem., Int. Ed. Engl.* **1996**, *35* (9), 989–991.
 (10) Ollivier, P. J.; DeBord, J. R. D.; Zapf, P. J.; Zubieta, J.; Meyer, L. M.; Wang, C.-C.; Mallouk, T. E.; Haushalter, R. C. *J. Mol. Struct.* **1998**, *470*, 49–60.
 (11) Shi, Z.; Zhang, L.; Zhu, G.; Yang, G.; Hua, J.; Ding, H.; Feng, S. *Chem. Mater.* **1999**, *11*, 3565–3570.
 (12) Zhang, L.; Shi, Z.; Yang, G.; Chen, X.; Feng, S. *J. Chem. Soc., Dalton Trans.* **2000**, 275–278.
 (13) Maggard, P. A.; Boyle, P. D. *Inorg. Chem.* **2003**, *42*, 4250–4252.
 (14) Liu, C.-M.; Gao, S.; Zhang, D.-Q.; Zhu, D.-B. *J. Coord. Chem.* **2005**, *58* (4), 327–334.
 (15) Xie, J.-Y.; Mao, J.-G. *J. Mol. Struct.* **2005**, *750*, 186–189.
 (16) Hargman, P. J.; Zubieta, J. *Inorg. Chem.* **2001**, *40*, 2800–2809.
 (17) Devi, R. N.; Rabu, P.; Golub, V. O.; O'Connor, C. J.; Zubieta, J. *Solid State Sci.* **2002**, *4*, 1095–1102.
 (18) Ueda, Y. *Chem. Mater.* **1998**, *10*, 2653–2664.
 (19) Lutta, S. T.; Chernova, N. A.; Zavalij, P. Y.; Whittingham, M. S. *J. Mater. Chem.* **2004**, *14*, 2922–2928.
 (20) Lutta, S. T.; Chernova, N. A.; Zavalij, P. Y.; Whittingham, M. S. *J. Mater. Chem.* **2003**, *13*, 1424–1428.
 (21) Kanada, M.; Harashina, H.; Tanaka, S.; Fukamachi, T.; Kobayashi, Y.; Sato, M. *J. Phys. Soc. Jpn.* **1998**, *67* (8), 2904–2909.
 (22) Zhang, Y.; Warren, C. J.; Haushalter, R. C.; Clearfield, A.; Seo, D.-K.; Whangbo, M.-H. *Chem. Mater.* **1998**, *10*, 1059–1064.
 (23) Yan, B.; Maggard, P. A. *Inorg. Chem.* **2006**, *45*, 4721–4727.
 (24) Maggard, P. A.; Yan, B.; Luo, J. *Angew. Chem., Int. Ed.* **2005**, *44*, 2553–2556.

- (25) Lin, H.; Yan, B.; Boyle, P. D.; Maggard, P. A. *J. Solid State Chem.* **2006**, *179*, 217–225.
 (26) Maggard, P. A.; Boyle, P. D. *Inorg. Chem.* **2003**, *42*, 4250–4252.
 (27) Yan, B.; Luo, J.; Greedan, J. E.; Maggard, P. A. *Inorg. Chem.* **2006**, *45*, 5109–5118.
 (28) Isobe, M.; Kagami, C.; Ueda, Y. *J. Cryst. Growth* **1997**, *181* (3), 314–317.
 (29) (a) Galy, J.; Darriet, J.; Hagenmuller, P. *Rev. Chim. Miner.* **1971**, *8* (3), 509–522. (b) Galy, J. *J. Solid State Chem.* **1992**, *100* (2), 229–245. (c) Isobe, M.; Ueda, Y. *J. Phys. Soc. Jpn.* **1996**, *65* (10), 3142–3145.

stoichiometric amount of Ag₂O in place of Cu(OH)₂. The reaction pouches were then loaded into the autoclave and heated to 230 °C for 3–5 days and allowed to radiatively cool to room temperature. Dark-red crystals with needle and plate morphologies were obtained in high purity (>99%) according to PXRD, with a mass percent yield of ~73% based on V.

Single-Crystal Structure Determination. A single-crystal X-ray data set of **I**, Cu(bpy)V₄O₁₀, was collected at 293 K on a Bruker-Nonius Apex2 CCD diffractometer using monochromatized Mo K α radiation ($\lambda = 0.71073$ Å). A black platelet crystal, with dimensions 0.24 × 0.03 × 0.10 mm, was fixed on a 20- μ m nylon loop with a small amount of immersion oil. The unit cell dimensions were determined from a symmetry-constrained fit of 5459 reflections within a 2θ range of 2.8–23.5°. The data collection strategy involved a combination of ψ and ω scans and the collection of frame exposures up to $2\theta_{\max} = 54.02^\circ$. The frame integrations were performed using *SAINTPPLUS* (57 655 reflections were processed, of which 3389 were unique),³⁰ and the raw data were corrected for Lorentz–polarization effects and for absorption using *SADABS*.³¹ The structure was solved and refined in the Bruker *SHELXTL*³² software package in the monoclinic space group $P2_1/c$, and the final space group assignment was confirmed using the software program *PLATON*.³³ The initial structure solution was obtained using direct methods, and the subsequent structure refinements were performed using a full-matrix least squares based on F^2 . H atoms were introduced in idealized positions and constrained to ride on the parent C positions. The final least-squares cycle was performed with the anisotropic refinement of all non-H atoms and which converged to $R1/wR2 = 0.048/0.128$ and a GOF = 1.06 for 2432 reflections ($I > 2\sigma$) and 245 independently refined parameters. Some data collection and refinement parameters for **I** are given in Tables 1 and 2, and selected interatomic distances are tabulated in Table 4.

Using procedures similar to those outlined above for **I**, a suitable single crystal of **II**, Ag(bpy)V₄O₁₀, with crystal dimensions of 0.15 × 0.08 × 0.05 mm, was characterized by X-ray diffraction with the following adjustments. The initial determination of the unit cell dimensions was calculated from a symmetry-constrained fit of 5919 reflections within a 2θ range of 2.8–25.2°, and the complete X-ray data collection included frame exposures out to $2\theta_{\max} = 51.72^\circ$. The structure was solved and anisotropically refined in the triclinic space group $P\bar{1}$, with the crystals exhibiting a problematic twinning that required application of the following twin law in the refinement: $[-1\ 0\ 0\ 0\ -1\ 0\ 0\ 0\ 1]$ (BASF = 0.056(2)). The final least-squares refinement cycle converged to $R1/wR2 = 0.079/0.211$ and a GOF = 1.03 for 2979 reflections ($I > 2\sigma$) and 246 independently refined parameters. Some data collection and refinement parameters for **II** are given in Tables 1 and 3, and selected interatomic distances are listed in Table 4.

Thermal Analysis. A TGA of each sample, 10.1 mg of **I** and 38.6 mg of **II**, was performed on a TGA Q50 analyzer, and the

- (30) *SAINTP-Plus Version 6.22 Data Processing for SMART System*; Bruker Analytical X-ray Instruments, Inc.: Madison, WI.
 (31) Sheldrick, G. M. *SADABS version 2.03, Software for Area Detector Absorption and Other Corrections*; Bruker Analytical X-ray Instruments, Inc.: Madison, WI.
 (32) Sheldrick, G. M. *SHELXTL NT version 6.10, Software Package for the Refinement of Crystal Structures*; Bruker Analytical X-ray Instruments, Inc.: Madison, WI.
 (33) (a) Spek, A. L. *PLATON—A Multipurpose Crystallographic Tool*; Utrecht University: Utrecht, The Netherlands. (b) Spek, A. L. *Acta Crystallogr., Sect. A* **1990**, *46*, C34.
 (34) (a) Brown, I. D.; Altermatt, D. *Acta Crystallogr., Sect. B* **1985**, *41*, 244–247. (b) Brese, N. E.; O’Keefe, M. *Acta Crystallogr., Sect. B* **1991**, *47*, 192–197.
 (35) Hormillosa, C. *Bond Valence Calculator*, version 2.00; McMaster University: Hamilton, Ontario, Canada, 1993.

Table 1. Selected Crystal and Refinement Data for M(bpy)V₄O₁₀ (**I**, M = Cu; **II**, M = Ag)

compd	I	II
fw	583.48	627.81
space group, Z	$P2_1/c$ (No. 14), 4	$P\bar{1}$ (No. 2), 2
temp, K	293	273
a, Å	3.6154(3)	3.5731(4)
b, Å	21.217(1)	10.429(1)
c, Å	20.267(1)	21.196(2)
α , deg	90	89.031(5)
β , deg	90.028(3)	89.322(5)
γ , deg	90	85.546(5)
V	1554.6(2)	787.3(2)
μ (Mo K α), mm ⁻¹	3.72	3.57
d_{calc} , g·cm ⁻³	2.49	2.65
reflns (total)	57 655	26 654
data/restraints/param	3389/0/245	2979/0/246
final R1, wR2 ^a [$I > 2\sigma(I)$]	0.048, 0.128	0.079, 0.211

$$^a R1 = \sum ||F_o| - |F_c|| / \sum |F_o|; wR2 = \{\sum [w(F_o^2 - F_c^2)^2] / \sum [w(F_o^2)^2]\}^{1/2}, w = \sigma_F^{-2}.$$

Table 2. Selected Atomic Coordinates and Equivalent Isotropic Displacement Parameters (Å²) for **I**

atom	x	y	z	U(eq) ^a
V1	0.2468(5)	0.53310(5)	0.71934(4)	0.0146(3)
V2	0.7455(5)	0.44227(5)	0.79289(4)	0.0156(3)
V3	0.7454(6)	0.49301(5)	0.93905(5)	0.0163(3)
V4	0.2492(6)	0.49067(5)	0.56049(5)	0.0171(3)
Cu	0.4997(3)	0.70741(5)	0.75227(4)	0.0333(3)
O1	0.748(2)	0.5056(2)	0.7215(2)	0.023(1)
O2	0.749(2)	0.4289(2)	0.8827(2)	0.020(1)
O3	0.254(2)	0.5417(2)	0.6294(2)	0.0180(9)
O4	0.255(2)	0.4918(2)	0.4627(2)	0.026(1)
O5	0.249(2)	0.4811(2)	0.9660(2)	0.025(1)
O6	0.244(2)	0.4710(2)	0.7916(2)	0.0198(9)
O7	0.252(2)	0.6042(2)	0.7459(2)	0.027(1)
O8	0.0260(2)	0.4208(2)	0.5875(3)	0.038(1)
O9	0.753(2)	0.5544(2)	0.8935(2)	0.032(1)
O10	0.752(2)	0.3740(2)	0.7610(2)	0.025(1)
N1	0.347(2)	0.7227(3)	0.8407(3)	0.020(2)
N2	0.694(3)	0.7190(3)	0.6660(3)	0.028(2)
C1	0.231(4)	0.6754(3)	0.8788(3)	0.027(2)
C2	0.099(2)	0.6857(3)	0.9428(3)	0.023(2)
C3	0.910(2)	0.7907(4)	0.5835(3)	0.027(2)
C4	0.782(3)	0.7776(3)	0.6455(3)	0.024(2)
C5	0.759(3)	0.6712(3)	0.6221(3)	0.024(2)
C6	0.875(2)	0.6817(3)	0.5593(3)	0.023(2)
C7	0.227(3)	0.7938(3)	0.9296(3)	0.020(2)
C8	0.352(2)	0.7818(4)	0.8666(3)	0.022(2)
C9	0.1044(2)	0.7456(3)	0.9707(3)	0.016(2)
C10	0.971(2)	0.7423(3)	0.5373(3)	0.016(2)

^a U(eq) is defined as one-third of the trace of the orthogonalized U_{ij} tensor.

data were plotted as the percent of starting weight versus temperature. The samples were heated to 500 °C at a rate of 2 °C·min⁻¹ under flowing O₂ gas (40 mL·min⁻¹). Post-TGA residues were characterized by PXRD in transmission mode on an Inel XRG 3000 diffractometer fitted with a CPS 120 position-sensitive detector and using Cu K α_1 radiation from a sealed-tube X-ray source.

Electrical and Magnetic Properties. Magnetic susceptibility measurements were taken for **I** (23.6 mg) and **II** (28.0 mg) on a Quantum Design MPMS XL SQUID magnetometer. In both cases, the magnetization was measured in the temperature range of 2–300 K at an applied field of 10 kG. The data were corrected for the diamagnetism of the sample holder and for the atomic cores using Pascal’s constants. Four-probe electrical conductivity measurements of **I** and **II** were taken on thin pellets using an MMR Technologies Hall and Van der Pauw Measurement System and a Joule-Thomson

Table 3. Selected Atomic Coordinates and Equivalent Isotropic Displacement Parameters (Å²) for **II**

atom	x	y	z	U(eq) ^a
Ag1	0.9860(4)	0.9469(1)	0.25214(5)	0.0393(4)
V1	0.7291(6)	0.5672(2)	0.2848(1)	0.0163(5)
V2	0.2739(6)	0.3913(2)	0.2080(1)	0.0166(5)
V3	0.2455(6)	0.4921(2)	0.0602(1)	0.0168(5)
V4	0.7597(6)	0.4867(2)	0.4404(1)	0.0174(5)
O1	0.758(2)	0.4677(9)	0.0349(4)	0.023(2)
O2	0.209(3)	0.6228(9)	0.0963(5)	0.031(2)
O3	0.273(2)	0.3741(8)	0.1214(4)	0.019(2)
O4	0.761(2)	0.448(1)	0.2098(4)	0.024(2)
O5	0.245(2)	0.511(1)	0.2837(4)	0.031(3)
O6	0.731(2)	0.5851(9)	0.3715(4)	0.020(2)
O7	0.800(3)	0.344(1)	0.4173(5)	0.035(2)
O8	0.247(2)	0.519(1)	0.4632(4)	0.025(2)
O9	0.695(3)	0.7116(9)	0.2589(4)	0.026(2)
O10	0.306(3)	0.2471(9)	0.2341(4)	0.028(2)
N1	0.807(3)	0.967(1)	0.1577(5)	0.022(2)
N2	0.174(3)	0.963(1)	0.3458(5)	0.026(3)
C1	0.693(4)	0.866(1)	0.1262(6)	0.026(3)
C2	0.583(4)	0.880(1)	0.0649(6)	0.023(3)
C3	0.569(4)	0.994(2)	0.0333(6)	0.027(3)
C4	0.680(4)	0.098(1)	0.0659(7)	0.023(3)
C5	0.793(4)	0.079(1)	0.1268(7)	0.027(3)
C6	0.234(4)	0.860(1)	0.3859(7)	0.026(3)
C7	0.361(4)	0.872(1)	0.4456(6)	0.025(3)
C8	0.430(4)	0.990(1)	0.4678(6)	0.021(3)
C9	0.359(4)	0.098(1)	0.4258(7)	0.021(3)
C10	0.232(4)	0.080(1)	0.3673(7)	0.030(3)

^a U(eq) is defined as one-third of the trace of the orthogonalized U_{ij} tensor.

Table 4. Selected Interatomic Distances (Å), Angles (deg), and Bond Valence Sums^a for M(bpy)V₄O₁₀ (**I**, M = Cu; **II**, M = Ag)

atom	atom	distance	atom	atom	distance	atom	atom	distance	
Compound I									
Cu1	N1	1.904(6)	V2	O1	1.975(4)	V4	O3	1.767(4)	
	N2	1.900(6)		O2	1.843(4)		O4	1.891(8)	
	O7	2.369(5)		O6	1.901(8)		O4	1.918(8)	
V1	O1	1.895(8)	V3	O6	1.914(7)	V-V distances	O4	1.983(4)	
	O1	1.905(8)		O10	1.587(4)		O8	1.580(5)	
	O3	1.832(4)		$\sum S_{ij} = 4.59$			$\sum S_{ij} = 5.06$		
	O6	1.970(4)		O2	1.777(4)		V1	V2	3.031(2)
	O7	1.602(4)		O5	1.894(8)		V1	V2	3.037(2)
	$\sum S_{ij} = 4.58$			O5	1.916(8)		V3	V3	3.057(3)
				O5	2.002(4)		V3	V3	3.094(3)
		O9	1.596(4)	V4	V4	3.068(3)			
		$\sum S_{ij} = 4.93$		V4	V4	3.076(3)			
Compound II									
Ag1	N1	2.11(1)	V2	O3	1.847(9)	V4	O6	1.770(9)	
	N2	2.12(1)		O4	1.881(9) (×2)		O7	1.57(1)	
	O1	2.74(1)		O5	2.05(1)		O8	1.869(9)	
V1	O4	2.034(9)	V3	O10	1.59(1)	V-V distances	O8	1.896(9)	
	O5	1.868(9)		$\sum S_{ij} = 4.56$			$\sum S_{ij} = 5.11$		
	O5	1.891(9)		O1	1.866(9)				
	O6	1.848(8)		O1	1.901(8)		V1	V2	3.046(3)
	O9	1.590(9)		O1	2.052(9)		V1	V2	3.048(3)
	$\sum S_{ij} = 4.59$			O2	1.57(1)		V4	V4	3.101(4)
				O3	1.771(8)		V3	V3	3.108(4)
		$\sum S_{ij} = 5.09$							

^a $S_{ij} = e^{[(R_0 - R)/B]}$, $B = 0.37$, and $R_0 = 1.784$ for V^V and 1.803 for V^{IV}.^{34,35}

refrigerator in the temperature range of 100–350 K. The pellets were 10 mm in diameter and formed from thoroughly ground powder samples that were pressed at ~9000 psi. Electrical contacts were deposited on the edge of the pellets using 0.003 in. manganin wires (MMR Technologies) and a Ag-containing epoxy resin.

Results and Discussion

Structural Descriptions. The two reduced hybrid vanadates, M(bpy)V₄O₁₀ (**I**, M = Cu⁺; **II**, M = Ag⁺; bpy = 4,4'-bipyridine), both exhibit novel 3D structures constructed from stacked vanadate layers [V₄O₁₀][−] that are coordinated to interlayer chains of [M(bpy)]⁺, as shown in Figure 1. The major structural differences between **I** and **II** arise from the relative orientations of the neighboring vanadate layers. In **I**, neighboring [V₄O₁₀][−] sheets are related by *c*-glide planes that invert the orientation of the apical O atoms, while the vanadate layers in **II** are simply stacked in an eclipsed fashion down the *b*-axis direction. The net result leads to a doubling of the unit cell dimension along the stacking direction in **I** [21.217(1) Å] compared to **II** [10.429(1) Å]. However, the interatomic distances across neighboring vanadate layers are ~0.2 Å longer for **I** than for **II**, although the Ag–O (2.739 Å) bonds connecting the layers are significantly longer than the Cu–O (2.369 Å) bonds. This apparent inconsistency is caused by the differences in the coordination geometries at the Cu⁺ and Ag⁺ sites and the resultant greater buckling of the Cu(bpy)⁺ chains for **I** (see below).

The vanadate layers, [V₄O₁₀][−], shown in Figure 2 (A and B for **I** and **II**, respectively), are topologically similar and consist of corner- and edge-shared VO₅ distorted tetragonal pyramids. Both layers are constructed from zigzag chains of edge-sharing VO₅ tetragonal pyramids, shown as the red and green polyhedra, and with neighboring chains connected via shared oxygen vertices into the full [V₄O₁₀][−] layers. There are four symmetry-unique V sites, two types within each of the red and green zigzag chains in Figure 2, each of which is coordinated via one short V–O apical bond at a distance of ~1.57–1.60 Å and four longer basal V–O bonds at distances of ~1.77–2.05 Å. These V–O distances are consistent with VO₅ tetragonal pyramids in prior known layered vanadate structures.^{9–17} The apical O atoms alternate in an “up–down” repeating pattern down the zigzag chains, and all are terminal except for a single set of apical O atoms on the green polyhedra that is also coordinated by Ag⁺/Cu⁺. The calculated bond valence sums are listed in Table 4 and indicate that two out of four symmetry-unique V atoms in each structure, V1 and V2 in each, have slightly reduced average valences of +4.56–4.59, while both V3 and V4 exhibit higher valences of +4.93–5.09. In addition to the one short V–O double bond for all V sites, the V3 and V4 sites in each structure have another relatively short V–O distance of ~1.77 Å, again reinforcing that these sites are preferentially 5+. The assignment of +4.5 for V1 and V2 in each structure is consistent with the formal charge on the [V₄O₁₀][−] layers, as is also confirmed by the magnetic properties (below). The reduction of vanadates by nitrogenous bases such as bipyridine is well documented in the literature.¹ The two types of zigzag chains shown in Figure 2 are drawn as red polyhedra for V⁵⁺ and as green polyhedra for V^{4.5+}. Thus, it shows that the chains of partially reduced VO₅ polyhedra are structurally isolated from each other. The V–V distances are shortest along the edge-shared VO₅

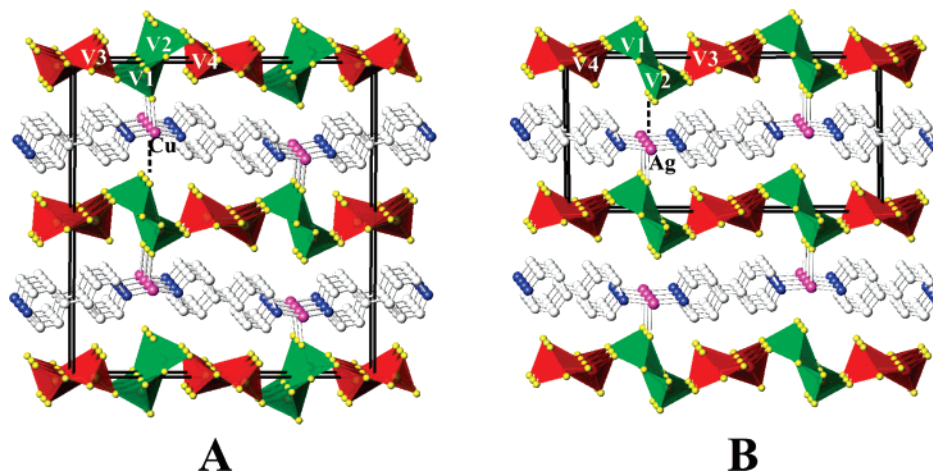


Figure 1. Structures of $\text{Cu}(\text{bpy})\text{V}_4\text{O}_{10}$ (A) and $\text{Ag}(\text{bpy})\text{V}_4\text{O}_{10}$ (B) viewed along the a direction, showing the vanadate $[\text{V}_4\text{O}_{10}]^-$ layers linked by the metal-organic $[\text{Cu}(\text{bpy})]^+$ or $[\text{Ag}(\text{bpy})]^+$ chains, respectively. The unit cells are outlined, and red polyhedra = V^{5+}O_5 , green = $\text{V}^{4.5+}\text{O}_5$, purple spheres = Ag or Cu, yellow = O, white = C, and blue = N.

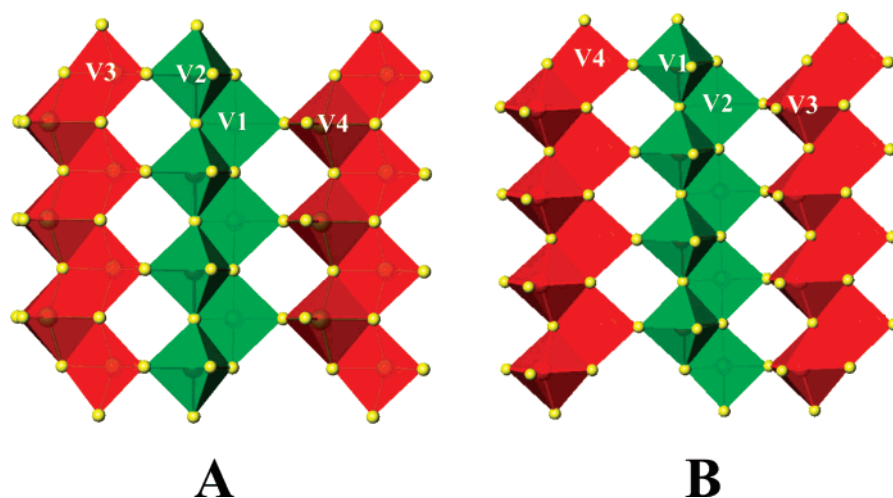


Figure 2. Sections of the vanadate layers of $\text{Cu}(\text{bpy})\text{V}_4\text{O}_{10}$ (A) and $\text{Ag}(\text{bpy})\text{V}_4\text{O}_{10}$ (B). Red polyhedra = V^{5+}O_5 , green = $\text{V}^{4.5+}\text{O}_5$, and yellow = O.

chains in the range of 3.03–3.11 Å and are slightly shorter for the reduced chains (~ 3.031 Å for **I** and ~ 3.046 Å for **II**) than for the normal-valent vanadate chains (~ 3.06 – 3.09 Å for **I** and ~ 3.10 Å for **II**).

Between the vanadate layers, the $\text{M}(\text{bpy})^+$ chains consist of Cu/Ag atoms each coordinated in a nearly linear fashion by bridging bpy ligands (Cu–N = ~ 1.90 Å and Ag–N = ~ 2.11 Å) and also to a single O atom of the vanadate layer [Ag–O = 2.74(1) Å and Cu–O = 2.369(5) Å] to form a roughly T-shaped to trigonal-planar geometry. The distances from Cu/Ag to the next-nearest O of the opposite $[\text{V}_4\text{O}_{10}]^-$ layer, shown as dashed lines in Figure 1 (A and B), are ~ 0.7 – 1.3 Å longer at $\text{Ag}\cdots\text{O} = 3.430$ Å and $\text{Cu}\cdots\text{O} = 3.659$ Å. Hence, in both **I** and **II**, the $\text{M}(\text{bpy})^+$ chains coordinate to the vanadate layers by one short Cu/Ag–O bond, alternately to the neighboring layer above and below, with the result that none of the red vanadate polyhedra and only one set of the green vanadate polyhedra have bonding interactions. Remarkably, the bpy ligands are oriented almost perpendicular to the vanadate layers (~ 78 – 83°), with neighboring bpy faces parallel to each other to give a short π – π stacking distance of ~ 3.3 – 3.4 Å and M–M distances

of ~ 3.57 – 3.62 Å. This ligand orientation also provides short favorable hydrogen-bonding interactions to the apical O atoms of the vanadate layer of ~ 2.34 – 2.70 Å. The aromatic rings of ligands typically lie flat over vanadate layers, such as is known in the related hybrids $\text{M}(\text{pyz})\text{V}_4\text{O}_{10}$ or $\text{Cu}(\text{pyz})_2\text{V}_6\text{O}_{16}\cdot x\text{H}_2\text{O}$.^{26,27} In **I**, the $\text{M}(\text{bpy})^+$ chains and vanadate layers are more buckled than those in **II**, resulting in an ~ 1.0 Å shorter c lattice dimension and an ~ 0.2 Å longer interlayer distance. This suggests that the coordination geometries and lengths of the $\text{M}(\text{bpy})^+$ chains have a significant impact upon the conformation of the vanadate layers.

The connectivity of vanadate polyhedra in **I** and **II** is identical, with the primary differences being the degree of buckling within the layers caused by the $\text{M}(\text{bpy})^+$ chains. Vanadate layers with similar polyhedral connectivities are also found in those reported for $(\text{MV})_{0.25}\text{V}_4\text{O}_{10}$ (MV = methylviologen) and $(4\text{-H}_2\text{NC}_5\text{H}_5\text{NH})\text{V}_2\text{O}_5$,³⁶ i.e., they contain zigzag chains of edge-shared VO_5 that link to neighboring chains via shared vertices. However, the vanadate layers

(36) (a) Bose, A.; He, P.; Liu, C.; Ellman, B. D.; Twieg, R. J.; Huang, S. D. *J. Am. Chem. Soc.* **2002**, *124*, 4–5. (b) Shan, Y.; Huang, R. H.; Huang, S. D. *Angew. Chem., Int. Ed.* **1999**, *38*, 1751–1754.

in **I** and **II** are more highly buckled compared to those in (MV)_{0.25}V₄O₁₀ and (4-H₂NC₅H₅NH)V₂O₅, which are nearly flat. For example, the V–O–V angles between neighboring zigzag chains are ~120.9–136° in **I** and **II**, compared to ~164.5° in the latter. Hence, the shared O vertices between neighboring zigzag chains exhibit a large degree of flexibility in their V–O–V angles, which can be modified by the interactions to the interlayer guest species. The vanadate layers in **I** and **II** are nearly isostructural with those in LiV₂O₅, which are also highly buckled but contain alternating chains of V⁴⁺ and V⁵⁺ polyhedra owing to its one additional electron per formula. The magnetic properties of LiV₂O₅ have been modeled according to a *S* = 1/2 Heisenberg antiferromagnetic linear chain.^{29c} However, while LiV₂O₅ contains interlayer Li⁺ ions, the structures of **I** and **II** have been modified by the different repeat distances and coordination preferences of the M(bpy)⁺ chains, which results in changes to the V–O–V angles and distances.

TGA. Hybrid oxide/organic solids can undergo ligand loss at relatively low temperatures to yield related condensed structures, such as is known for M(py_z)V₄O₁₀ or CuReO₄(py_z).^{27,37} This relatively soft collapse of the inorganic layers can also represent a convenient low-temperature pathway to parent compositions that can be difficult to synthesize otherwise, such as for CuReO₄. To probe the thermal structural evolution of **I** and **II**, each sample was heated to 500 °C in flowing O₂ and the resulting residues were characterized by PXRD. The TGA of each sample (see the Supporting Information) exhibited two closely-spaced weight losses, for a net of 26.4% for **I** at 350–400 °C and 25.6% for **II** at 400–450 °C, which is consistent with the complete removal of bpy ligands (calcd 26.7% for **I** and 24.9% for **II**). These results were consistent with PXRD measurements on the black TGA residues, which matched well with the patterns simulated for Cu_{0.94}V₄O₁₀ and Ag_{0.8}V₄O₁₀ (Supporting Information).^{38,39} Further, these have structural features relatively similar to those described for **I** and **II** but are typically synthesized at higher temperatures of >600 °C. Neither excess Ag nor Cu could be detected in the PXRD. At the highest temperatures of ~450 °C, the sharp weight losses are followed by a relatively slower weight gain (~2.7% for Ag and ~2% for Cu), showing that the vanadate layers are first reduced by bpy and then subsequently oxidized by O₂, as was also observed for M(py_z)V₄O₁₀. For example, in Ag(bpy)V₄O₁₀, a total weight loss of 28.3% is observed by 450 °C, corresponding with the loss of one bpy and one O atom per formula (calcd 27.4%). Next, the temperature rapidly (3–10 s) dropped to ~375 °C and was then followed by a relatively slow 2.7% weight gain over the next 2–3 h for a net weight loss of 25.6%. A similar weight loss behavior is also observed for Cu(bpy)V₄O₁₀.

Electrical and Magnetic Properties. The chemical formulas of both **I** and **II** are consistent with one electron added

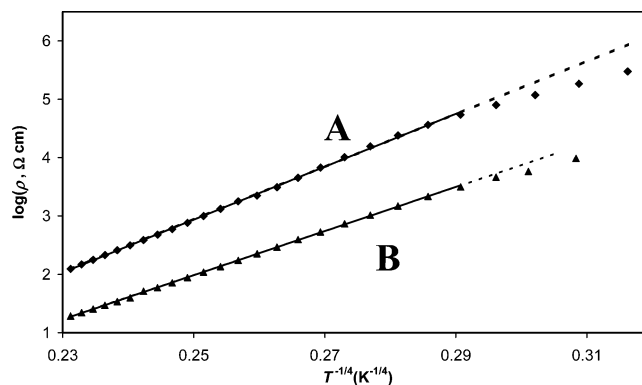


Figure 3. Temperature dependence of the electrical conductivity of (A) Cu(bpy)V₄O₁₀ and (B) Ag(bpy)V₄O₁₀ versus $T^{-1/4}$. The solid lines show the fit to $\rho = \rho_0 \exp(T_0/T)^{1/4}$.

(or reducing) per four V atoms, for which the bond valence sums (above and Table 4) show are averaged over two out of four V atoms (i.e., V^{4.5+}). Both electrical and magnetic properties were measured as a function of the temperature to probe for the degree of electron localization and exchange coupling as is known in the condensed version of these reduced layered vanadates, i.e., in LiV₂O₅. Their electrical conductivities both exhibit a positive temperature dependence that is consistent with semiconducting behavior. However, the nonlinear relationship of log(ρ) versus 1/*T* (Supporting Information) indicates that the thermally activated hopping is not characterized by a constant activation energy over this temperature range. Thus, the electrical conductivity was modeled according to Mott's variable-range-hopping (VRH) equation $\rho = \rho_0 \exp(T_0/T)^n$ (where ρ_0 and T_0 are fitting constants and *n* can be either 1/2, 1/3, or 1/4).⁴⁰ This VRH model of the conductivity describes the energetically favorable electron hopping as also occurring between more remote V sites rather than solely nearest-neighbor V sites. As shown in Figure 3, the conductivity for both **I** and **II** exhibited a best fit ($R^2 > 0.9995$) to Mott's equation with $n = 1/4$, before beginning to diverge at the lowest temperatures. Thus, the VRH model suggests the hopping of randomly localized electrons across the entire vanadate layer, rather than restricted solely to the edge-shared zigzag chains of V^{4.5+} (green polyhedra). This behavior is an interesting contrast to that in M(py_z)V₄O₁₀ (*M* = Co, Ni, Zn), which has only one symmetry-inequivalent V^{4.5+} and an electron-hopping mechanism consistent with a single activation energy, although a VRH conduction behavior has been observed in other condensed strontium and barium vanadates.⁴¹

The magnetic susceptibilities of **I** and **II**, plotted in Figure 4, both show a strong temperature dependence and are consistent with a random localization of the unpaired electrons. The data at higher temperatures could be fitted to a Curie–Weiss expression with $\theta = -25$ and -31 K and $C = 0.40$ emu·mol⁻¹·K (Table 5) for both **I** and **II**, respec-

(37) Lin, H.; Maggard, P. A. *Inorg. Chem.* **2007**, *46*, 1283–1290.

(38) Savariault, J.-M.; Deramond, E.; Galy, J. Z. *Kristallogr.* **1994**, *209*, 405–412.

(39) Deramond, E.; Savariault, J.-M.; Galy, J. *Acta Crystallogr., Sect. C* **1994**, *50*, 164–166.

(40) (a) Mott, N. F. *Philos. Mag.* **1976**, *34* (4), 643–645. (b) Mott, N. F. *Metal–Insulator Transitions*; Taylor & Francis: London, 1974.

(41) (a) Niu, H.; Fukushima, N.; Ando, K. *Phys. Rev. B* **1991**, *44* (9), 4724–4726. (b) Bridges, C. A.; Greedan, J. E. *J. Solid State Chem.* **2004**, *177*, 1098–1110.

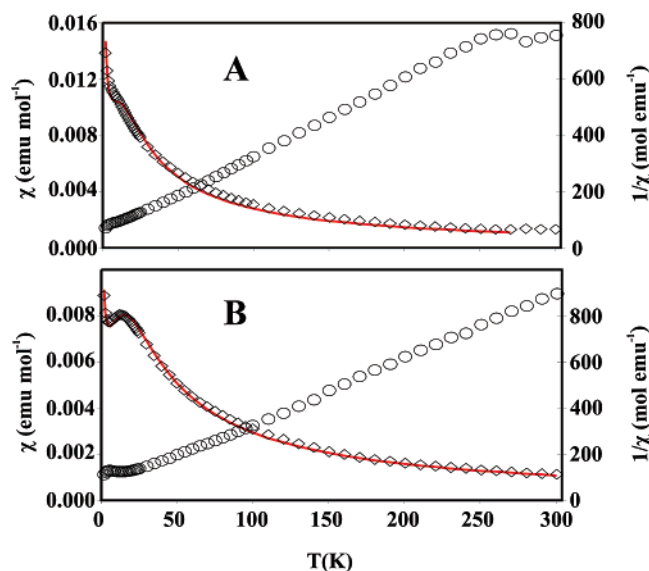


Figure 4. Magnetic susceptibility of (A) Cu(bpy)V₄O₁₀ and (B) Ag(bpy)V₄O₁₀. Red lines are the fit to the Heisenberg linear antiferromagnetic chain model. The magnetic susceptibility for Ag(bpy)V₄O₁₀ reaches a maximum at $T = 12$ K.

Table 5. Fitting Parameters for the Magnetic Susceptibility of M(bpy)V₄O₁₀ (I, M = Cu; II, M = Ag) According to the Curie–Weiss and Heisenberg Linear Antiferromagnetic Chain Models

	I	II
	Curie–Weiss Model	
temp range, K	12–250	18–300
R^2 ^a	0.999	0.997
C , emu	0.40	0.40
Θ , K	–25	–31
	Heisenberg Antiferromagnetic Chain Model ^b	
R^2 ^a	0.992	0.998
g	1.81(2)	1.90(1)
J , cm ^{–1}	–6.8(2)	–9.01(8)
p , impurity %	3.6(2)	1.50(2)

^a $R^2 = \sum(X_i - X_o)^2 / \sum(Y_i - X_o)^2$, where X_i = predicted, Y_i = measured, and X_o = average. ^b $\chi = (Ng^2\beta^2/kT)(A/B)$, where $A = 0.25 + 0.14995X + 0.30094X^2$, $B = 1.0 + 1.9862X + 0.68854X^2 + 6.0626X^3$, and $X = |J|/kT$.⁴¹

tively. The Curie constants are close to that expected for one unpaired spin per formula ($C = 0.374$ emu·mol^{–1}·K). However, at the lowest temperatures, the χ – T plots exhibit a change in curvature, most significantly for **II** with a maximum value at around 12 K. Accordingly, a more complete modeling of the magnetic data could be achieved using the Heisenberg linear antiferromagnetic chain model for V⁴⁺ with $S = 1/2$ and taking into account the presence of monomeric paramagnetic impurities with concentration p ,⁴² listed in Table 5. A least-squares refinement of the fitting

parameters gave a best fit for **I** and **II** of $g = 1.81(2)$ and $1.90(1)$, $J = -6.8(2)$ and $-9.01(8)$ cm^{–1}, and $p = 0.036(2)$ and $0.015(2)$, shown plotted as red lines in Figure 4. These results suggest a gradual localization of the electrons along isolated vertex-shared chains of VO₅ pyramids at the lowest temperatures, as known in LiV₂O₅. It is interesting to consider that this pattern of electron localization could be driven by the coordination of the Cu⁺/Ag⁺ ions to the single set of (green) VO₅ polyhedra, which accounts for one out of every four V sites. However, further low-temperature structural and magnetic data are necessary to more fully elucidate the origins of these magnetic properties.

Conclusions

Two new hybrid vanadates, M(bpy)V₄O₁₀ (M = Cu⁺, Ag⁺), have been synthesized via hydrothermal methods and structurally characterized to have closely related structures containing layers of Ag(bpy)⁺ or Cu(bpy)⁺ chains that alternate with partly reduced V₄O₁₀[–] layers. The vanadate layer in each is constructed from zigzag chains of edge-shared VO₅ tetragonal pyramids, with neighboring chains alternately containing V^{4.5+} and V⁵⁺ ions. The bpy ligands can be removed from each by heating to ~350–400 °C to yield the purely inorganic M₂V₄O₁₀ solids. Their electrical conductivities follow Mott’s VRH model, while the magnetic susceptibilities at the lowest temperatures can be fitted to the Heisenberg linear antiferromagnetic chain model. Both represent some of the first hybrid layered vanadates that are closely related to reduced vanadates that constitute interesting quantum-spin systems with more extended spin lattices. These also serve to illustrate that the interlayer guest species have a significant influence on the vanadate layers and therefore on the electron exchange between V atoms.

Acknowledgment. Support from a Beckman Young Investigator Award (to P.A.M.) from the Beckman Foundation and a CAREER Award (to P.A.M.) from the National Science Foundation (Grant DMR-0644833) and assistance with the collection of single-crystal X-ray data (P. Boyle) are gratefully acknowledged.

Supporting Information Available: Crystallographic data in CIF format, TGA data, PXRD of TGA residues, and conductivity data for both **I** and **II**. This material is available free of charge via the Internet at <http://pubs.acs.org>.

IC700729Q

(42) (a) Hatfield, W. E. *J. Appl. Phys.* **1981**, *52* (3), 1985–1990. (b) Estes, W. E.; Gavel, D. P.; Hatfield, W. E.; Hodgson, D. J. *Inorg. Chem.* **1978**, *17*, 1415–1421.